Preparation of Mesoporous Pd/Si_3N_4 Nanocomposites as Heterogeneous Catalysts via Three Different Chemical Routes

Fei Cheng,[†] Stephen M. Kelly,*,[†] Nigel A. Young,*,[†] Chris N. Hope,[†] Katie Beverley,[†]
M. Grazia Francesconi,[†] Stephen Clark,[†] John S. Bradley,[†] and Frédéric Lefebvre[‡]

Department of Chemistry, The University of Hull, Cottingham Road, Hull, HU6 7RX, United Kingdom, and Laboratoire de Chimie Organométallique de Surface, 43 Boulevard du 11 Novembre 1918, 69616 Villeurbanne Cedex, France

Received May 11, 2006. Revised Manuscript Received August 7, 2006

Mesoporous palladium/silicon nitride nanocomposites were prepared via three different chemical routes to generate simultaneous control of the solid-state morphology of the palladium nanoparticles and that of the silicon nitride support at the same time as controlling the pore size and size distribution. Pyrolysis of the reaction product of silicon diimide gel with $PdCl_2$ under a NH_3 flow at 1000 °C gave a composite with highly crystalline Pd nanoparticles dispersed in an α-Si_3N_4 matrix. A composite with partially crystallized Pd nanoparticles dispersed in an amorphous Si_3N_4 matrix was obtained by the hydrogen reduction of the reaction product of silicon nitride with $PdCl_2$, whereas hydrogen reduction of an impregnated mixture of Si_3N_4 with bis(dibenzylideneacetone)palladium (DBA) led to the formation of a composite with amorphous Pd nanoparticles dispersed in an amorphous Si_3N_4 matrix. Most of these new mesoporous nanocomposites exhibit a high surface area >400 m^2 g^{-1} and a narrow pore size distribution of 5−12 nm with a loading of up to 2% Pd nanoparticles 2−20 nm in diameter. Preliminary investigations show that these nanocomposites are potentially useful heterogeneous catalysts for a range of liquid-phase chemical reactions.

Introduction

Transition-metal-loaded porous materials are currently of interest because of their potential applications in heterogeneous catalysis, selective gas adsorption, catalytic gas filters, and many other areas.[1−3] Porous metal oxides, such as SiO_2, Al_2O_3, and zeolites, are usually used as inorganic supports for the active phases.[1,2,4] However, metal oxides usually exhibit a relatively low thermal conductivity and instability at high temperatures, mainly because of sintering of the active metal with the support. In contrast, silicon nitride exhibits high thermal conductivity and low creep. It is hard, strong, and exhibits low chemical reactivity, e.g., to corrosion and oxidation, even at high temperature. This combination of properties renders silicon nitride useful as a dense, high-temperature ceramic.[5−7] However, some initial reports suggest silicon nitride could be a very useful support for catalytically active phases.[8−12] These reports describe reactions carried out in the gas phase, i.e., the oxidation of methane using Pd/Si_3N_4 and Pt/Si_3N_4,[8−10] the selective hydrogenation of butadiene to butene using Pd/Si_3N_4,[11] and the dehydrogenation of propane using Pt/Si_3N_4.[12] The surface area of the catalysts used varied from very low ($S = 2-66$ m^2 g^{-1}) for commercial Si_3N_4 to moderately low ($S < 100$ m^2 g^{-1}) for Si_3N_4 prepared by a gas-phase method. The phase and morphology of the silicon nitride support, i.e., amorphous or crystalline Si_3N_4 and the ratio of crystalline forms (α-Si_3N_4 and β-Si_3N_4) were found to influence the catalytic effectiveness of these nanocomposites in the oxidation of methane.[10] However, although it was found that crystalline α-Si_3N_4 appeared to be the most effective form of the support for catalytic activity, it appeared that mechanical instability and oxidation of amorphous Si_3N_4 at the high temperatures used to carry out the oxidation may be responsible for the low activity.[10] The Pd/Si_3N_4 catalyst showed good selectivity in the partial hydrogenation of butadiene to butene.[11] Unfortunately, the activity of the catalyst reduced quite quickly to a low steady state and so the percentage conversion was relatively low.[11]

---

[*] Corresponding author. E-mail: s.m.kelly@hull.ac.uk (s.m.k.).
[†] The University of Hull.
[‡] Laboratoire de Chimie Organométallique de Surface.

(1) Che, M.; Clause, O.; Marcilly, Ch. In *Handbook of Heterogeneous Catalysis*; Ertl, G., Knözinger, H., Weitkamp, J., Eds.; Wiley−VCH: Weinheim, Germany, 1997, Vol. 1.
(2) Nicholas, F. S.; Prabir, K. D. *Sens. Actuators, B* **2003**, *88*, 168.
(3) Kolyma, S.; Nakashima, H.; Sugahara, Y.; Kuroda, K. *Chem. Lett.* **1998**, 191.
(4) Toebes, M. L.; van Dillen, J. A.; de Jong, K. P. *J. Mol. Catal. A: Chem.* **2001**, *173*, 75.
(5) Boberski, C.; Hamminger, R.; Peuckert, M.; Aldinger, F.; Dillinger, R.; Heinrich, J.; Huber, J. *Angew. Chem., Int. Ed.* **1989**, *28*, 1560.
(6) Baldus, H. P.; Jansen, M. *Angew. Chem., Int. Ed.* **1997**, *36*, 329.
(7) Kroke, E.; Li, Y. L.; Konetschny, C.; Lecomte, E.; Fasel, C.; Riedel, R. *Mater. Sci. Eng., R* **2000**, *26*, 97.
(8) Méthivier, C.; Massardier, J.; Bertolini, J. C. *Appl. Catal., A* **1999**, *182*, 337.
(9) Monnet, F.; Schuurman, Y.; Cadete Santos Aires, F. J.; Bertolini, J. C.; Mirodatos, C. *Catal. Today* **2001**, *64*, 51.
(10) Kurzina, I.; Cadete Santos Aires, F. J.; Bergeret, G.; Bertolini, J. C. *Chem. Eng. J.* **2005**, *107*, 45.
(11) Garcia, G.; Cadete Santos Aires, F. J.; Bertolini, J. C. *J. Catal.* **2003**, *214*, 26.
(12) Hullmann, D.; Wendt, G.; Singliar, U.; Ziegenbalg, G. *Appl. Catal., A* **2002**, *225*, 261.

10.1021/cm061106h CCC: $33.50

Scheme 1. Three General Methods Used to Prepare Mesoporous Silicon Nitride Doped with Palladium Nanoparticles

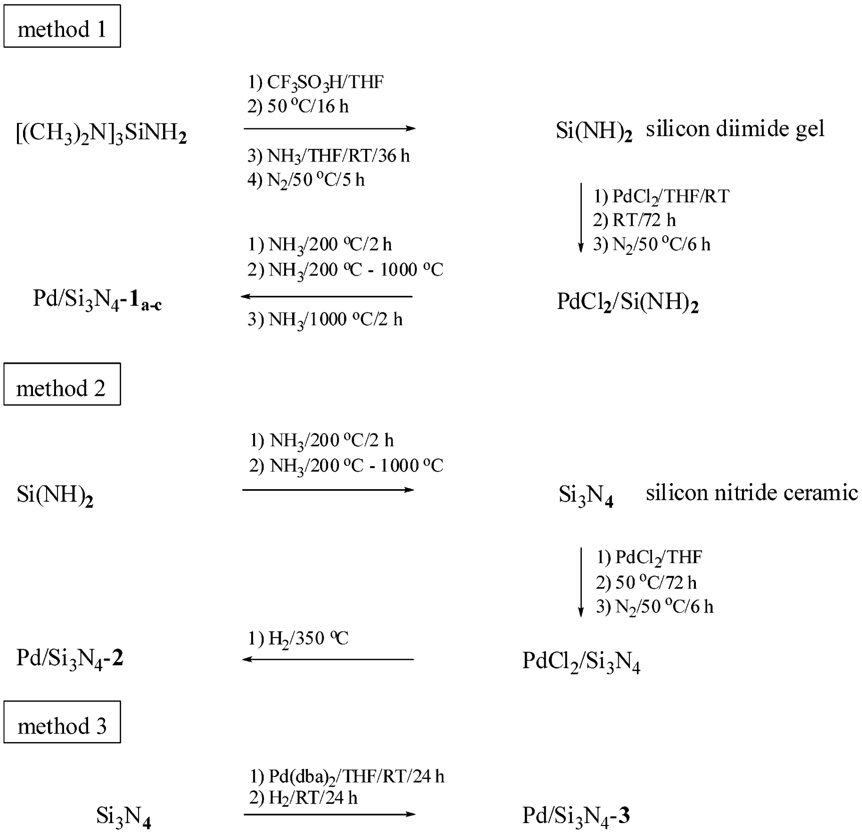

We have pioneered the chimie douce sol−gel preparation of a high surface area mesoporous silicon diimide gel, $Si(NH)_x(NH_2)_y(NMe_2)_z$ [Me = CH_3], by acid-catalyzed ammonolysis of *tris*(dimethylamino)silylamine, $(Me_2N)_3SiNH_2$, often referred to by the acronym TDSA.[13] Pyrolysis of the silicon diimide gel (abbreviated to $Si(NH)_2$) at 1000 °C gives a mesoporous amorphous silicon nitride with high surface area and narrow pore size distribution.[14] We have also successfully prepared high-surface-area multinary imidosilicates containing boron or aluminum as the metals. Three gels with different silicon:boron molar ratios were prepared by the acid-catalyzed ammonolysis of the single source precursors $B[NHSi(NMe_2)_3]_3$,[15] $B_3[NHSi(NMe_2)_3]_3N_3H_3$,[16,17] and $(NMe_2)B_3[NHSi(NMe_2)_3]_2N_3H_3$,[17] respectively. Silicon aluminum imide gel was prepared by the acid-catalyzed ammonolysis of the single-source precursor $Si_3Al(NH)_x(NH_2)_y(NMe_2)_z$.[18] Pyrolysis of these gels at 1000 °C under a NH_3 flow led to the formation of mesoporous silicon boron nitride and silicon aluminum nitride composites.[14,16,17] Preliminary results of investigation of the use of the silicon boron nitride and silicon nitride ceramics derived from the mesoporous gels prepared from $B[NHSi(NMe_2)_3]_3$ and *tris*(dimethylamino)silylamine, respectively, indicate that they can be formed into stable mesporous membranes and used as efficient selective gas filters in solid-state gas sensor applications.[19−21] This synthetic flexibility, simplicity and control over the ceramic morphology suggested that our nonaqueous sol−gel approach to synthesising mesoporous silicon nitride with a large surface area and narrow pore size distribution could be applicable to the preparation of effective M/Si_3N_4 catalysts incorporating transition metal nanoparticles, such as palladium, for gas-phase reactions and reactions in solution requiring heterogeneous catalysts.[22] Several other important sol−gel routes to nitrides have been reported, which may also be used to prepare highly porous materials, e.g., boron nitride,[23−27] metal

---

(13) Rovai, R.; Lehmann, C. W.; Bradley, J. S. *Angew. Chem., Int. Ed.* **1999**, *38*, 2036.
(14) Cheng, F.; Clark, S.; Kelly, S. M.; Bradley, J. S.; Lefebvre, F. *J. Am. Ceram. Soc.* **2004**, *87*, 1413.
(15) Cheng, F.; Toury, B.; Lefebvre, F.; Bradley, J. S. *Chem. Commun.* **2003**, 242.
(16) Cheng, F.; Toury, B.; Archibald, S. J.; Bradley, J. S. *J. Organomet. Chem.* **2002**, *657*, 71.
(17) Cheng, F.; Archibald, S. J.; Clark, S.; Toury, B.; Kelly, S. M.; Bradley, J. S.; Lefebvre, F. *Chem. Mater.* **2003**, *15*, 4651.
(18) Cheng, F.; Kelly, S. M.; Lefebvre, F.; Clark, S.; Supplit, R.; Bradley, J. S. *J. Mater. Chem.* **2005**, *15*, 772.
(19) Maisonat, A.; Delprat, H.; Baumbach, M.; Schütze, A.; Cheng, F.; Kelly, S. M.; Parret, F.; Menini, P.; Soulantica, K.; Chaudret, B. *Technical Digest of Eurosensors XVIII*, Rome, Italy, Sept 12−15, 2004.
(20) Baumbach, M.; Schütze, A.; Cheng, F.; Kelly, S. M.; Delprat, H.; Parret, F.; Menini, P.; Soulantica, K.; Chaudret, B.; Maisonat, A. *Proceedings of the IEEE Sensors Conference 2004*, Vienna, Austria, Oct 25−27, 2004.
(21) Cheng, F.; Kelly, S. M.; Clark, S.; Bradley, J. S. *J. Membr. Sci.* **2006**, online.
(22) Cheng, F.; Kelly, S. M.; Young, N. A.; Clark, S.; Francesconi, M. G.; Lefebvre, F.; Bradley, J. S. *Chem. Commun.* **2005**, *45*, 5662.
(23) Narula, C. K.; Schaeffer, R.; Datye, A.; Paine, R. T. *Inorg. Chem.* **1989**, *28*, 4053.
(24) Paine, R. T.; Narula, C. K.; Schaeffer, R.; Datye, A. K. *Chem. Mater.* **1989**, *1*, 486.
(25) Narula, C. K.; Lindquist, D. A.; Min Fan, M.; Borek, Th. T.; Duesler, E. N.; Datye, A. K.; Schaeffer, R.; Paine, R. T. *Chem. Mater.* **1990**, *2*, 377
(26) Lindquist, D. A.; Borek, Th. T.; Kramer, S. J.; Narula, C. K.; Johnston, G.; Schaeffer, R.; Smith, D. M.; Paine, R. T. *J. Am. Ceram. Soc.* **1990**, *73*, 757.

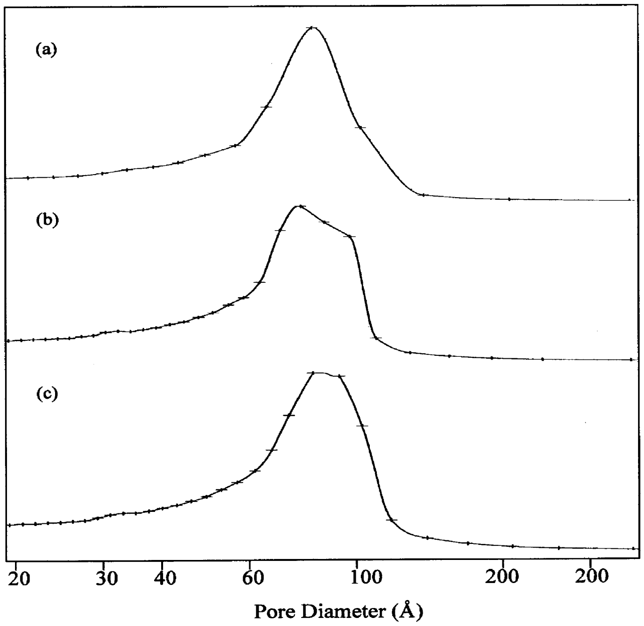

Figure 1. Pore size distribution of (a) silicon diimide gel ($Si(NH)_2$), (b) doped silicon diimide gel 5%-$PdCl_2/Si(NH)_2$ and (c) doped silicon diimide gel 2%-$PdCl_2/Si(NH)_2$.

(carbo)nitrides,[28−33] silicon carbonitride,[34−40] and boron carbonitride.[41,42]

In this paper, we now report three practical and efficient chemical approaches using nonaqueous sol−gel chemistry for the preparation of mesoporous silicon nitride nanocomposites incorporating palladium nanoparticles as potential heterogeneous catalysts, see Scheme 1. The three different routes facilitate chemical control of the nanocomposite components crystal morphology (amorphous/crystalline) and macroscopic structural morphology (size, density, and dispersity of the pores). We also describe initial investigations of the catalytic activity of these novel nanocomposites for a range of chemical reactions and attempts to establishpreliminary correlations between catalytic activity and nanoparticle/Si_3N_4 morphology.

Experimental Section

General Comments. All procedures were performed under an anhydrous nitrogen atmosphere using standard Schlenk techniques or in a nitrogen-filled glove box. The solvent tetrahydrofuran (THF) was freshly distilled from sodium/benzophenone prior to use. Trifluoromethanesulfonic acid and liquified ammonia were obtained from Sigma Aldrich and Energas LTD, respectively. *Tris*(dimethylamino)silylamine $(Me_2N)_3SiNH_2$ (TDSA)[13] and *bis*(dibenzylideneacetone)palladium $Pd(DBA)_2$ were prepared according to previously reported procedures.[13,43] Fourier transform infrared spectra were recorded on a Nicolet Magna-500 FTIR spectrometer. ^{29}Si cross-polarization (CP) spectra with magic-angle spinning (MAS) were obtained with a Bruker DSX-300 spectrometer operating at frequencies of 59.6 MHz with a chemical shift related to tetramethylsilane (TMS). X-ray diffraction analysis was carried out using a SIEMENS D5000 instrument. Nitrogen adsorption isotherms were performed at 77 K using a Micromeritics TriStar 3000 instrument, and surface area was determined from BET analysis. The amounts of palladium in the composite were determined by an inductively coupled plasma Perkin-Elmer 40 emission ICP instrument. Palladium K-edge EXAFS spectra were collected in transmission mode on samples at ca. 80 K diluted in BN on stations 9.2 and 9.3 of the Daresbury Laboratory Synchrotron Radiation Source operating at 2 GeV with circulating currents of 100−250 mA. On station 9.2, harmonic rejection was achieved by detuning the monochromator to 60%, whereas a mirror was used on station 9.3. The data were calibrated using the PAXAS program[44] by setting the midpoint of the first peak in the first derivative of Pd foil to 24350.0 eV. Background subtraction was carried out using the Daresbury Laboratory implementation of Spline.[45] The EXAFS data were fitted using curved wave theory within EXCURV98.[46] Transmission electron microscopy (TEM) was performed on a JEOL 2011 electron microscope operating at an accelerating voltage of 120 kV. The samples were prepared using carbon-coated copper grids. One drop of an ethanol suspension of the sample was placed on the carbon-coated grid using a microsyringe. GC-MS was performed on a QP505A Schimadzu with electron impact (EI) at a source temperature of 200 °C.

Method 1. **Preparation of Mesoporous Pd/Si_3N_4 Composites (Pd/Si_3N_4−1a/1b/1c) via Pyrolysis of a Reaction Product of Silicon Diimide Gel with $PdCl_2$.** Trifluoromethanesulfonic acid (86 μL, 97 mmol) was added to a solution of TDSA (17.09 g, 97 mmol) in dry THF (700 cm^3) in a 2000 cm^3 round-bottomed three-necked flask. After being heated at 50 °C for 16 h, the solution was allowed to cool to room temperature. A solution of ammonia (0.39 g, 22.8 mmol) in cold THF (6 cm^3) was added. After being left quiescent at room temperature for 18 h, ammonia gas was bubbled through the reaction mixture for 10 min. The resulting mixture was left standing at room temperature for another 18 h to give a rigid gel. Evaporation of the solvent and evolved dimethylamine in a stream of nitrogen followed by drying under reduced

---

(27) Borek, Th. T.; Qiu, Xi.; Rayfuse, L. M.; Datye, A. K.; Paine, R. T.; Allard, L. F. *J. Am. Ceram. Soc.* **1991**, *74*, 2587.

(28) Pfennig, B. W.; Bocarsly, A. B.; Prud'homme, R. K. *J. Am. Chem. Soc.* **1993**, *115*, 2661.

(29) Heibel, M.; Kumar, G.; Wyse, C.; Bukovec, P.; Bocarsly, A. B. *Chem. Mater.* **1996**, *8*, 1504.

(30) Sharp, S. L.; Bocarsly, A. B.; Scherer, G. W. *Chem. Mater.* **1998**, *10*, 825.

(31) Deshpande, R. S.; Sharp-Goldman, S. L.; Willson, J. L.; Bocarsly, A. B.; Gross, J.; Finnefrock, A. C.; Gruner, S. M.; *Chem. Mater.* **2003**, *15*, 4239.

(32) Vondrova, M.; Klimczuk, T.; Miller, V. L.; Kirby, B. W.; Yao, N.; Cava, R. J.; Bocarsly, A. B. *Chem. Mater.* **2005**, *17*, 6216.

(33) Vondrova, M.; Majsztrik, P. W.; Gould, S.; Bocarsly, A. B. *Chem. Mater.* **2005**, *17*, 4755.

(34) Gabriel, A. O.; Riedel, R. *Angew. Chem., Int. Ed.*. **1997**, *36*, 384.

(35) Gabriel, A. O.; Riedel, R.; Stork, S.; Maier, W. F. *Appl. Organomet. Chem.* **1997**, *11*, 833.

(36) Riedel, R.; Kroke, E.; Greiner, A.; Gabriel, A. O.; Ruwisch, L.; Nicolich, J.; Kroll, P. *Chem. Mater.* **1998**, *10*, 2964.

(37) Gabriel, A. O.; Riedel, R.; Dressler, W.; Reichert, S.; Gervais, Ch.; Maquet, J., and Babonneau, F. *Chem. Mater.* **1999**, *11*, 412.

(38) Kim, D. S.; Kroke, E.; Riedel, R.; Gabriel, A. O.; Shim, S. C. *Appl. Organomet. Chem.* **1999**, *13*, 495.

(39) Nahar-Borchert, S.; Kroke, E.; Riedel, R.; Boury, B.; Corriu, R. J. P. *J. Organomet. Chem.* **2003**, *686*, 127.

(40) Volger, K. W.; Hauser, R.; Kroko, E.; Riedel, R.; Ikuhara, Y. H.; Iwamoto, Y. *J. Ceram. Soc. Jpn.* **2006**, *114*, 567.

(41) Kroke, E.; Völger, K. W.; Klonczynski, A.; Riedel, R. *Angew. Chem., Int. Ed.* **2001**, *40*, 1698.

(42) Völger, K. W.; Kroke, E.; Gervais, Ch.; Saito, T.; Babonneau, F.; Riedel, R.; Iwamoto, Y.; Hirayama, T. *Chem. Mater.* **2003**, *15*, 755.

(43) Takahashi, Y.; Ts Ito, Sakai, S.; Ishii, Y. *Chem. Commun.* **1970**, 1065.

(44) Binsted, N. *PAXAS, Program for the Analysis of X-ray Absorption Spectra*; University of Southampton: Southampton, U.K., 1998.

(45) *EXSPLINE, A Program for EXAFS Background Subtraction*; Daresbury Laboratory: Chesire, U.K., 2000. Based on an original program: Ellis, P. Ph.D. Thesis, *SPLINE*, University of Sydney, Sydney, Australia, 1995.

(46) Binsted, N. *EXCURV98, CCLRC Daresbury Laboratory Computer Program*; CCLRC, Daresbury Laboratory: Chesire, U.K., 1998.

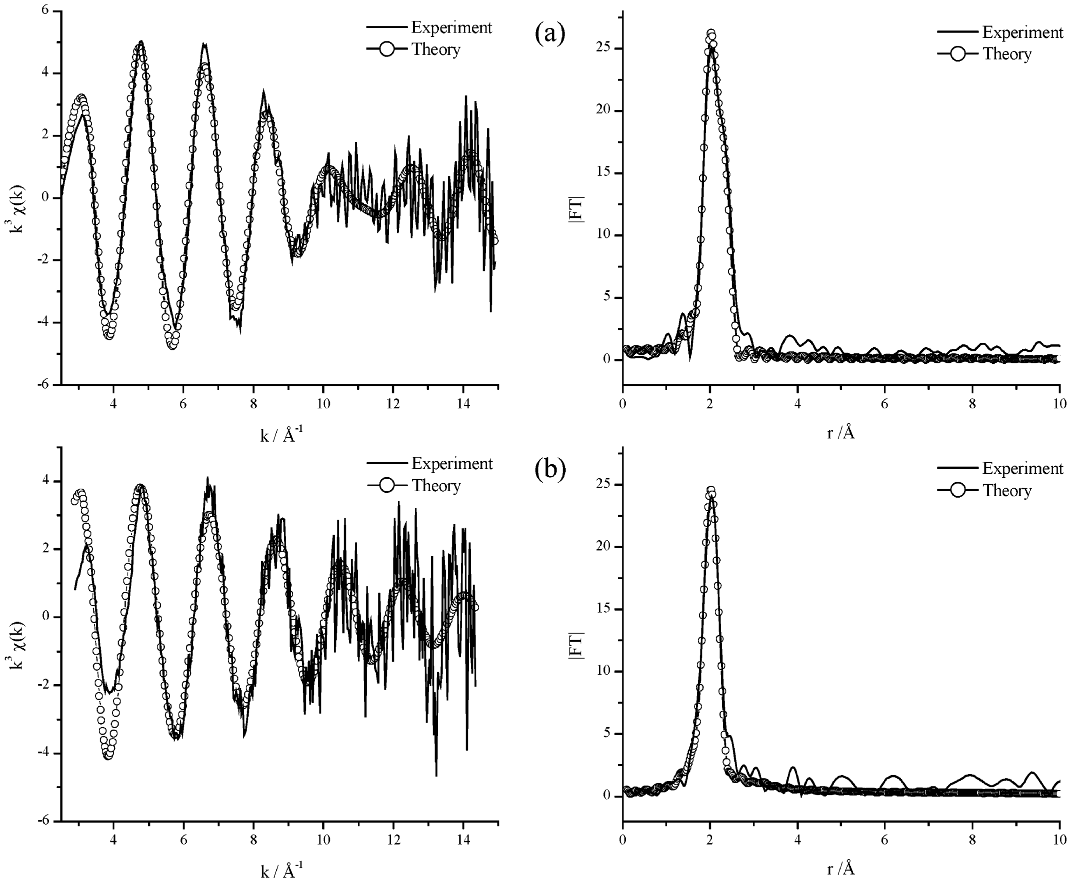

Figure 2. Pd K-edge EXAFS (left) and FTs (right) at ca. 80 K for (a) 5%-PdCl$_2$/SiNH$_2$ and (b) 2%PdCl$_2$/SiNH$_2$.

Table 1. Refined EXAFS Parameters for 5%-PdCl$_2$/Si(NH)$_2$ and 2%-PdCl$_2$/Si(NH)$_2$

	r (Å)	2σ^2 (Å^2)	E_f (V)	*R* (%)	FI
		5%PdCl$_2$/Si(NH)$_2$			
Pd−Cl (×1)	2.296(7)	0.0055(8)	−0.7(7)	34.0	0.59
Pd−N (×3)	2.050(5)	0.0062(11)			
		2%PdCl$_2$/Si(NH)$_2$			
Pd−N (×4)	2.053(5)	0.0102(13)	−2.3(12)	50.2	1.45

pressure at 50 °C for 5 h gave a translucent white silicon diimide gel.[13] PdCl$_2$ in 20 cm^3 dry THF was then added to the silicon diimide gel (Si(NH)$_2$) to give a loading of either 5 or 2% PdCl$_2$:gel (w/w). Each of the resulting mixtures was stirred at room temperature for 72 h. Evaporation of THF by a stream of nitrogen and then drying under reduced pressure at 50 °C for 6 h yielded two yellow powders, 5%-PdCl$_2$/Si(NH)$_2$ and 2%-PdCl$_2$/Si(NH)$_2$, which were then pyrolyzed in a tube furnace to yield the ceramic products Pd/Si$_3$N$_4$−**1a**, −**1b**, and −**1c**. About 0.5 g of the precursor gel complex 5%-PdCl$_2$/Si(NH)$_2$ or 2%-PdCl$_2$/Si(NH)$_2$ was placed in a BN boat, which was then introduced into a quartz tube in a glove box. The quartz tube was removed from the glove box and connected with NH$_3$ flow. The precursor gel complex 5%-PdCl$_2$/Si(NH)$_2$ or 2%-PdCl$_2$/Si(NH)$_2$ was heated to 200 °C and held at 200 °C for 2 h; it was then heated at 5 °C min^{-1} to 1000 °C and held at this temperature for 2 h under a NH$_3$ flow to yield the nanocomposite ceramics Pd/Si$_3$N$_4$−**1a** and −**1b**. A similar pyrolysis of **5**%-PdCl$_2$/Si(NH)$_2$ at a heating rate of 2 °C min^{-1} yielded the ceramic Pd/Si$_3$N$_4$−**1c**.

Method 2. Preparation of Mesoporous Pd/Si$_3$N$_4$ Composites (Pd/Si$_3$N$_4$−2) via Pyrolysis of a Reaction Product of Silicon Nitride with PdCl$_2$. About 0.5 g of silicon diimide gel (Si(NH)$_2$) was placed in a BN boat, which was then introduced into a quartz tube in a glove box. The quartz tube was removed from the glove box and connected with a NH$_3$ flow. The gel was heated to 200 °C, held at that temperature for 2 h, and then heated at 5 °C min^{-1} to 1000 °C under a current of NH$_3$ to yield mesoporous Si$_3$N$_4$. About 5% PdCl$_2$ (PdCl$_2$:Si$_3$N$_4$, w/w) and 20 cm^3 dry THF were then added to the cooled silicon nitride powder prepared in this way. The resulting mixture was stirred at 50 °C for 72 h and then cooled to room temperature; the solid material was filtered off, washed with dry THF, and then dried under reduced pressure at 50 °C for 6 h to give a yellow powder PdCl$_2$/Si$_3$N$_4$. The complex PdCl$_2$/Si$_3$N$_4$ was pyrolyzed in a tube furnace. About 0.5 g of complex PdCl$_2$/Si$_3$N$_4$ was placed in a BN boat, which was then introduced into a quartz tube in a glove box. The quartz tube was removed from the glove box and connected with 8% H$_2$−Ar flow. The complex PdCl$_2$/Si$_3$N$_4$ was heated to 350 °C for 4 h to yield a brown ceramic solid Pd/Si$_3$N$_4$−**2** with 1.7% palladium content.

Method 3. Preparation of Mesoporous Pd/Si$_3$N$_4$ Composites via an Impregnation Method (Pd/Si$_3$N$_4$−3). A solution of *bis*(dibenzylideneacetone)palladium Pd(DBA)$_2$[47,48] (0.016 g) in dry THF (8.1 cm^3) was added to a suspension of Si$_3$N$_4$ (0.30 g) in THF (20 cm^3) according to modified literature methods.[10,11,47,48] The resulting mixture was stirred at room temperature for 24 h in an autoclave and then 25 psi (1.7 bar) of hydrogen was introduced into the system and stirred at room temperature for another 24 h. After removal of the solvent under reduced pressure, the solid was washed three times with dichloromethane and then dried under reduced pressure to yield a gray ceramic powder Pd/Si$_3$N$_4$−**3**.

Hydrogenation Experiments. The catalytic reactions were carried out in a stainless steel Parr autoclave fitted with a pressure

---

(47) Duteil, A.; Quaue, R.; Chaudret, B.; Mazel, R.; Roucau, C.; Bradley, J. S. *Chem. Mater.* **1993**, *5*, 341.

(48) Dominguez-Quintero, O.; Martinez, S.; Henriquez, Y.; D'Ornelas, L.; Krentzien, H.; Osuna, J. *J. Mol. Catal. A: Chem.* **2003**, *197*, 185.

Table 2. Refined Pd K-edge EXAFS Data for the Reduction Products Pd/Si_3N_4−1c, Pd/Si_3N_4−2, and Pd/Si_3N_4−3 and Pd Foil

	Pd/Si_3N_4−**1**						
	Pd−Pd (×12)	Pd−Pd (×6)	Pd−Pd (×24)	Pd−Pd (×12)	E_f (V)	R (%)	FI
r_{Pd-Pd} (Å)	2.745(6)	3.932(24)	4.761(13)	5.490(set to $2r_1$)	−2.59	43.5	1.77
$2\sigma^2$ ($Å^2$)	0.0101(7)	0.0115(41)41	0.0119(18)17	0.0155(31)			
	Pd/Si_3N_4−**2**						
	Pd−Pd (×12)	Pd−Pd (×6)	Pd−Pd (×24)	Pd−Pd (×12)	E_f (V)	R (%)	FI
r_{Pd-Pd} (Å)	2.743(6)	3.889(37)	4.752(16)	5.486 (set to $2r_1$)	−1.73	38.9	1.71
$2\sigma^2$ ($Å^2$)	0.0104(7)	0.0156(68)	0.0137(23)	0.0153(29)			
	Pd/Si_3N_4−**3**						
	Pd−Pd (×4.3)				E_f (V)	R (%)	FI
r_{Pd-Pd} (Å)	2.755(6)				3.6(18)	49.0	1.34
$2\sigma^2$ ($Å^2$)	0.0102(2)						
	bulk Pd						
	Pd−Pd (×12)	Pd−Pd (×6)	Pd−Pd (×24)	Pd−Pd (×12)	E_f (V)	R (%)	FI
r_{Pd-Pd} (Å)	2.748(2)	3.878(9)	4.769(5)	5.496 (set to $2r_1$)	−4.33	20.99	0.22
$2\sigma^2$ ($Å^2$)	0.0051(2)	0.0076(17)	0.0083(7)	0.0093(8)			

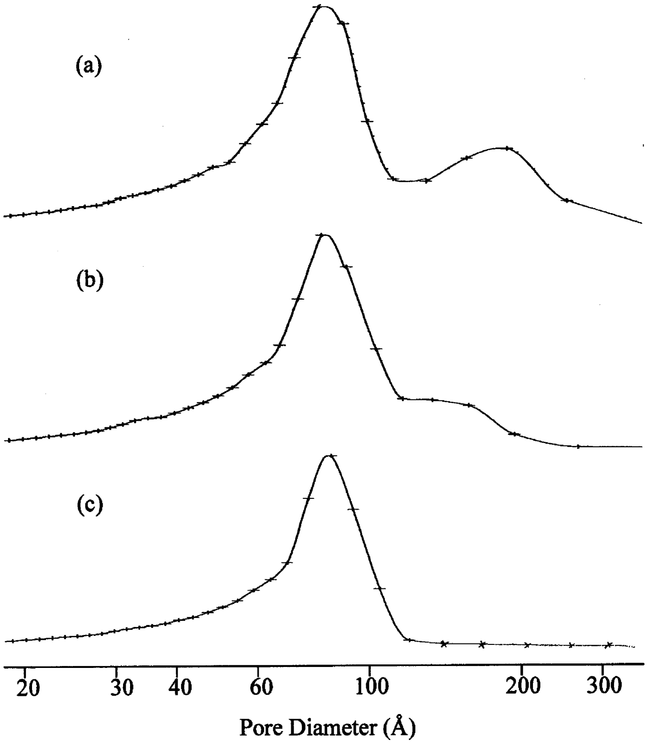

Figure 3. Pore size distribution of (a) ceramic product Pd/Si_3N_4−**1a** formed by pyrolysis of 5%-$PdCl_2$/$Si(NH)_2$ at 5 °C min^{-1}, (b) ceramic product Pd/Si_3N_4−**1b** formed by pyrolysis of 2%-$PdCl_2$/$Si(NH)_2$ at 5 °C min^{-1}, and (c) ceramic product Pd/Si_3N_4−**1c** formed by pyrolysis of 5%-$PdCl_2$/$Si(NH)_2$ at 2 °C min^{-1}.

gauge. The catalyst/substrate ratio was calculated according to the Pd concentration in the Pd/Si_3N_4 nanocomposite. The reaction mixtures were analyzed by GC-MS. All the hydrogenations using the catalyst Pd/Si_3N_4−**1c**, −**2**, or −**3** or cyclohexanone were carried out in a similar fashion to allow comparisons with similar reactions carried out with palladium nanoclusters on silica supports (Pd/SiO_2) to be made.[48]

Typical Experiment. The composite Pd/Si_3N_4−**3** (0.012 g, 0.83% Pd content) was introduced into the autoclave, 2 cm^3 (16.1 mmol) 1-hexene was added, and H_2 was introduced to 40 psi (2.76 bar); the autoclave was then heated to 30 °C in an oil bath. After reaction for 4 h, the reaction mixture was allowed to cool to room temperature, the pressure was released, and the reaction mixture was analyzed.

Results and Discussion

Method 1. The silicon diimide gel used to prepare the mesoporous Pd/Si_3N_4 composites (Pd/Si_3N_4−**1a**, −**1b**, and **1c**) was prepared by a modification of our previously reported method.[13] However, although IR and ^{29}Si and ^{13}C CP-MAS NMR analyses indicated that the gel contained a considerable amount of residual dimethylamino groups $Si(NH)_x(NH_2)_y$-(NMe_2), the silicon diimide gel is abbreviated as $Si(NH)_2$ in the manuscript for simplicity. Physisorption analysis showed that the gel exhibits a mesoporous structure with a high surface area (1032 m^2 g^{-1}) and narrow pore size distribution (5−12 nm).

Nitrogen physisorption analysis indicated that the intermediate gel complexes 5%-$PdCl_2$/$Si(NH)_2$ and 2%-$PdCl_2$/$Si(NH)_2$ also exhibit a mesoporous structure. The pore size distribution is very similar to that of the silicon diimide gel, see Figure 1, but the surface area has decreased to 814 and 845 m^2/g for the gel complexes 5%-$PdCl_2$/$Si(NH)_2$ and 2%-$PdCl_2$/$Si(NH)_2$, respectively. The decrease in surface area, compared to the original undoped gel ($Si(NH)_2$), suggests that some of the palladium is located within the pores of the gel and is blocking some of them. Another possible explanation could be that the higher concentration of $PdCl_2$ leads to a different degree of crosslinking and/or a different morphology on a nanoscale as a result of catalytic action of the palladium species during the gelation, aging, and calcination processes.

Because the gel has many functional groups Si−NH_2, Si−NH, and Si−NMe_2, reaction of ≡SiNH_2 groups with $PdCl_2$ will give ≡SiNH−Pd−Cl type species (eq I). In addition, the resulting ≡SiNH−Pd−Cl may react with another ≡SiNH_2 to form a ≡SiNH−Pd−NHSi≡ group (eq II). Pd K-edge EXAFS shows that the doped gel complex 5%-$PdCl_2$/$Si(NH)_2$ has Pd−Cl and Pd−N distances of 2.30(3) and 2.05(3) Å, respectively (Figure 2 and Tables 1 and 2). There is no evidence for Pd−Pd distances at ca. 3.4 Å observed in both $PdCl_2(NH_3)_2$ and $PdCl_2(en)$, indicating that the Pd is most likely dispersed throughout the $Si(NH)_2$ gel rather than

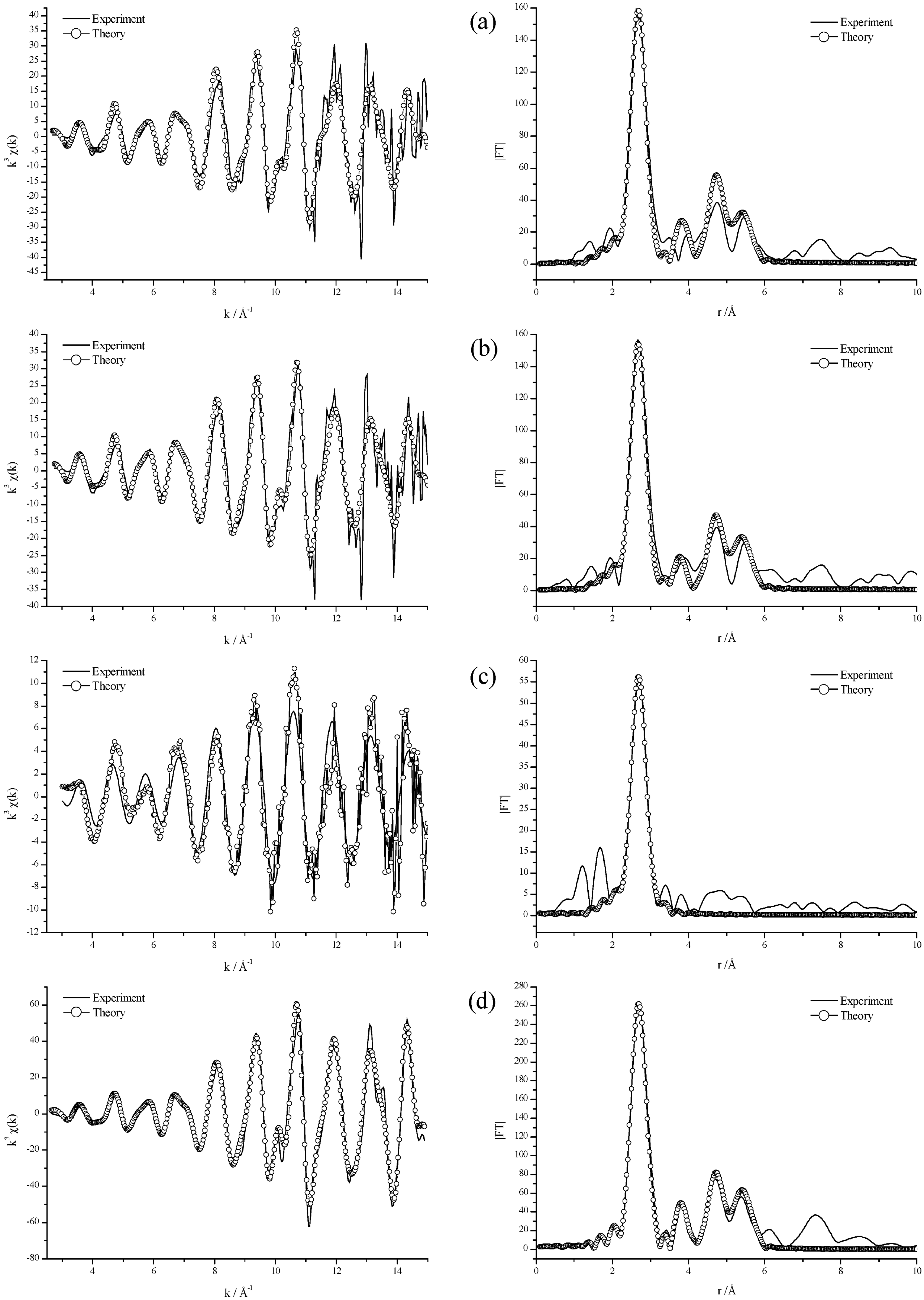

Figure 4. Pd K-edge EXAFS (left) and FTs (right) at ca. 80 K of the reduction products (a) Pd/Si$_3$N$_4$−**1c**, (b) Pd/Si$_3$N$_4$−**2**, and (c) Pd/Si$_3$N$_4$−**3**; (d) bulk palladium.

being in localized aggregates. The best fit to coordination numbers for the doped gel complex 5%-PdCl$_2$/Si(NH)$_2$ is for a “PdClN$_3$” type complex. However, the doped gel complex 2%-PdCl$_2$/Si(NH)$_2$ has only 4 Pd−N at 2.05(3) Å,

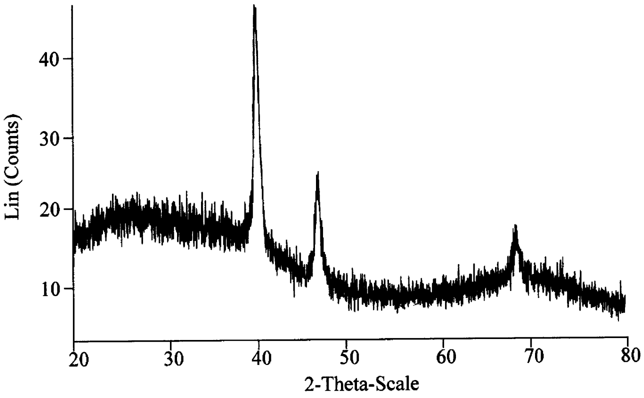

Figure 5. XRD pattern of the product Pd/Si_3N_4−**2** prepared by heating $PdCl_2$/Si_3N_4 at 350 °C under 8% H_2−Ar.

with no evidence of any Pd−Cl interactions present in the gel (Figure 2 and Table 1). The Pd atoms in ≡SiNH−Pd−Cl and/or ≡SiNH−Pd−NHSi≡ are then most likely coordinated with two further N-containing groups to give a 4-coordinate square planar geometry expected for Pd(II). These results indicate that with 2% $PdCl_2$, all the Pd−Cl sites have been reacted with the gel in 2%-$PdCl_2$/Si$(NH)_2$ because of reactions I and II, whereas with 5% $PdCl_2$, only part of the ≡SiNH−Pd−Cl groups reacted with another ≡$SiNH_2$ to form ≡SiNH−Pd−NHSi≡ species in the 5%-$PdCl_2$/Si$(NH)_2$ gel. Although these interpretations correlate best with the EXAFS data, it must be remembered that it is an averaging structural technique, so there is probably a distribution of species with two, one, and no chlorine atoms attached to the Pd, with the gel surface N functional groups providing both the atoms and charge balance to maintain square-planar Pd(II).

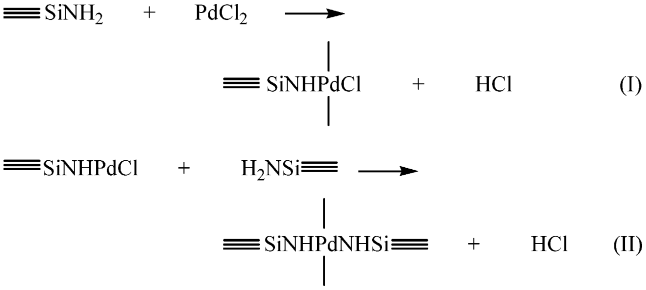

$$\equiv SiNH_2 + PdCl_2 \longrightarrow \equiv SiNH\overset{|}{\underset{|}{Pd}}Cl + HCl \quad (I)$$

$$\equiv SiNHPdCl + H_2NSi\equiv \longrightarrow \equiv SiNH\overset{|}{\underset{|}{Pd}}NHSi\equiv + HCl \quad (II)$$

Pyrolysis of the gel complexes 5%-$PdCl_2$/Si$(NH)_2$ and 2%-$PdCl_2$/Si$(NH)_2$ by heating from 200 to 1000 °C at 5 °C min^{-1} under a NH_3 flow yielded the ceramic products Pd/Si_3N_4−**1a** and Pd/Si_3N_4−**1b**, respectively. A pore size distribution at 50−120 Å (see Figure 3), which is very similar to that of the gel complex 5%-$PdCl_2$/Si$(NH)_2$, is observed. Unfortunately, a second pore size distribution is also observed at 150−250 Å for the ceramic products Pd/Si_3N_4−**1a** and Pd/Si_3N_4−**1b**, which may be due to partial decomposition and rearrangement of the network of intermediates during the pyrolysis process.[22] Pyrolysis of the gel complex 5%-$PdCl_2$/Si$(NH)_2$ by heating from 200 to 1000 °C at a lower heating rate, i.e., 2 °C min^{-1} under a NH_3 flow, gave a mesoporous ceramic Pd/Si_3N_4−**1c** with only one pore size distribution at 50−120 Å, which is very similar to that of the precursor gel complex 5%-$PdCl_2$/Si$(NH)_2$. ICP analysis for the composite Pd/Si_3N_4−**1c** indicated a content of palladium of 2.2%. The Pd K-edge EXAFS spectrum of Pd/Si_3N_4−**1c** is very similar to that of bulk Pd (Figure 4), with essentially identical interatomic distances, but lower intensity oscillations in the EXAFS and peaks in the FT. Despite these lower intensities, the first shell coordination number refined to ca. 12, as did that for bulk Pd, but with slightly larger Debye−Waller factors. This, together with similar relative intensities of the other peaks in the FTs, indicates the presence of Pd particles where the average Pd environment is very similar to that in bulk Pd, although the larger Debye−Waller factors indicate greater disorder than in bulk Pd. Previous work[49] indicates that this behavior is consistent with relatively large Pd particles with a small surface fraction. Although it has been proposed that the relative ratios of the first and third shell can be used to define the cluster size,[49b] it is clear from the FTs that this is very similar in both Pd/Si_3N_4−**1c** and bulk Pd, indicating Pd clusters with diameters no smaller than 5 nm. The presence of small Pd particles (5−10 nm) dispersed in the α-Si_3N_4 matrix was supported by XRD and TEM analyses.[22] All the ceramic products Pd/Si_3N_4−**1a**, −**1b**, and −**1c** have high surface areas (≥400 m^2 g^{-1}).

Method 2. Preparation of Mesoporous Pd/Si_3N_4 Composites (Pd/Si_3N_4−2) via Pyrolysis of a Reaction Product of Silicon Nitride with $PdCl_2$. The XRD pattern of the doped silicon nitride ceramic Pd/Si_3N_4−**2** indicates the formation of partially crystallized palladium,[50] but unlike Pd/Si_3N_4−**1a**, −**1b**, and −**1c** discussed above, no crystallized α-Si_3N_4 was found (see Figure 5). Nitrogen adsorption analysis shows that the composite material exhibits a mesoporous structure with a surface area of 403 m^2 g^{-1} and a pore size distribution similar to that of silicon nitride (see Figure 6).

The Pd K-edge EXAFS spectrum of Pd/Si_3N_4−**2** is essentially identical to that of Pd/Si_3N_4−**1c** and is very similar to that of bulk Pd (Figure 4), with very similar interatomic distances, but slightly larger Debye−Waller factors. The first shell coordination number refines to 12, and although the larger Debye−Waller factors indicate greater disorder than in bulk Pd, the EXAFS data are consistent with small Pd particles where the average Pd environment is similar to that in bulk Pd, indicating that the surface fraction is small. Previous work[49] indicates that this behavior is consistent with Pd particles with diameters greater than 5 nm. The TEM image shows nanosize (5−20 nm) Pd particles on the surface of silicon nitride (see Figure 7), supporting the result of EXAFS.

Method 3. Preparation of Mesoporous Pd/Si_3N_4 Composites via an Impregnation Method (Pd/Si_3N_4−3). The IR spectrum of the doped silicon nitride ceramic Pd/Si_3N_4−**3** shows a big broad peak centered at 950 cm^{-1} and a small broad peak centered at 3425 cm^{-1}, see Figure 8, which can be attributed to the ν(Si−N) and ν(N−H) absorptions,

---

(49) (a) Frenkel, A. I.; Hills, C. W.; Nuzzo, R. G.; *J. Phys. Chem. B* **2001**, 105, 12689. (b) Jentys, A. *Phys. Chem. Chem. Phys.* **1999**, *1*, 4059. (c) Benfield, R. E. *J. Chem. Soc., Faraday Trans.* **1992**, 88, 1107.

(50) *Powder Diffraction Data File*, 01-076.-1407 (for α-Si_3N_4) and 03-065.-2867 (for Pd metal); JCPDS International Center for Diffraction Data: Swathmore, PA, 2003.

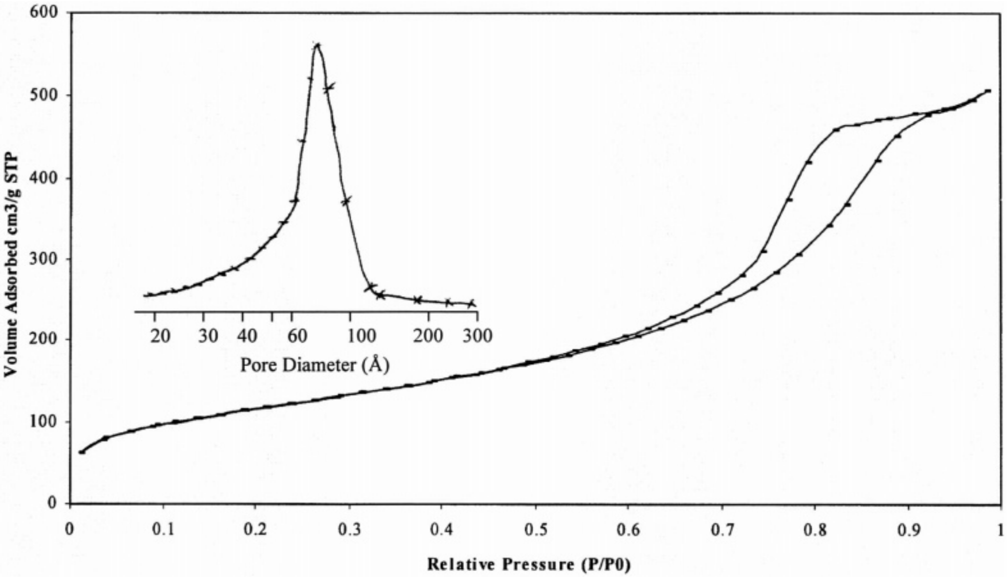

Figure 6. Nitrogen adsorption and desorption isotherms of the product Pd/Si$_3$N$_4$−**2** prepared by heating PdCl$_2$/Si$_3$N$_4$ at 350 °C under 8% H$_2$−Ar.

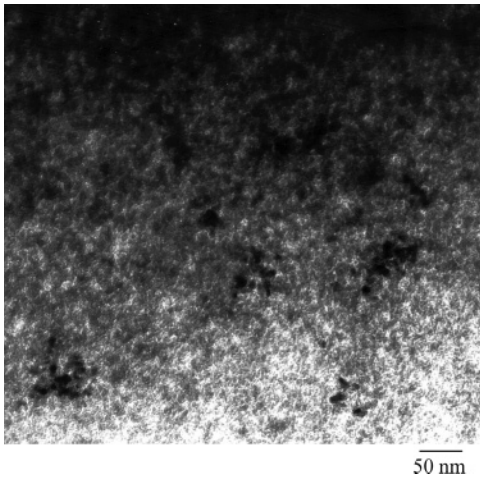

Figure 7. TEM image of the product Pd/Si$_3$N$_4$−**2** prepared by heating PdCl$_2$/Si$_3$N$_4$ at 350 °C under 8% H$_2$−Ar.

respectively.[51] The organic groups in Pd(dba)$_2$ have been removed during the reduction reaction at 350 °C. XRD analysis showed that both the Si$_3$N$_4$ and Pd are amorphous. Although the Pd content is low (0.83% as indicated by ICP analysis) and the EXAFS (see Figure 4) spectrum was fairly noisy, it is clear in comparison to that of Pd/Si$_3$N$_4$−**1c** and Pd/Si$_3$N$_4$−**2** as well as bulk Pd at the same temperature (ca. 80 K) that both the intensity of the EXAFS oscillations in Pd/Si$_3$N$_4$−**3** and their complexity are much lower. This is mirrored in the FTs, where, for the reduction product of Pd(dba)$_2$/Si$_3$N$_4$, there is a single feature with about a fifth of the intensity of the first peak in the FT of bulk Pd and a third of the intensity in Pd/Si$_3$N$_4$−**1c** and Pd/Si$_3$N$_4$−**2**. The Pd−Pd distance of 2.75(3) Å is in good agreement with that of bulk Pd (2.75(3) Å), but the occupation number refines to about 4.3, compared to 12.2 for bulk Pd. The relative weakness of the outlying shells means they were not included in the refinement. This behavior is entirely consistent with the presence of small and amorphous Pd particles within the ceramic, with a significant number of the Pd atoms located at the surface. Previous work[49] indicates that the particle size is probably on the order of 1−2 nm in this case.

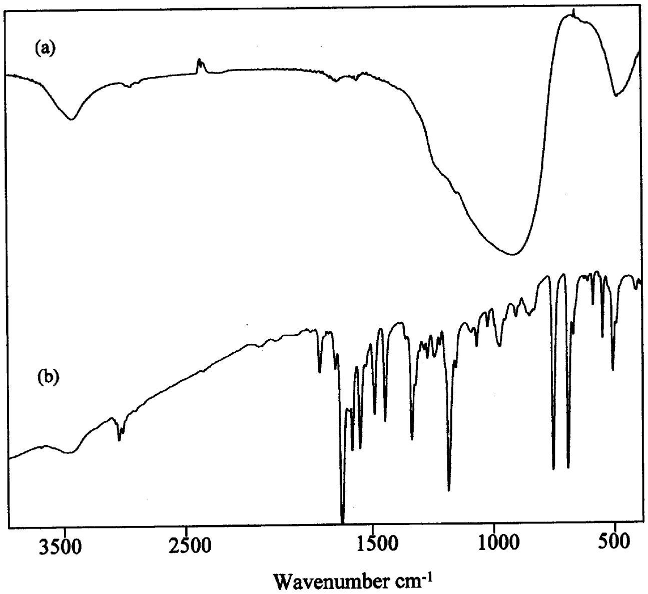

Figure 8. IR spectra of (a) the reduction product Pd/Si$_3$N$_4$−**3** formed by reduction of the complex Pd(DBA)$_2$/Si$_3$N$_4$ and (b) the organometallic precursor Pd(DBA)$_2$.

Nitrogen adsorption analysis shows that the ceramic Pd/Si$_3$N$_4$−**3** exhibits a mesoporous structure with pore size distribution very similar to that of Si$_3$N$_4$ (see Figures 9 and 10). The BET surface area is 346 m^2 g^{-1}, which is lower than that of the original Si$_3$N$_4$.

The TEM micrograph shown in Figure 11 shows that aggregates (5−10 nm) containing very small metal particles (1−2 nm as confirmed by EXAFS) are dispersed in the Si$_3$N$_4$ support.

Catalysis. A limited number of reactions were chosen to demonstrate the catalytic activity of the Pd/Si$_3$N$_4$−**1c**, −**2**, and −**3** mesoporous ceramics prepared by methods 1−3 (Table 3). The nanoclusters found in Pd/Si$_3$N$_4$−**1c** and Pd/Si$_3$N$_4$−**2** prepared by methods 1 and 2, respectively, exhibit

---

(51) Nakamoto, K. *Infrared and Raman Spectra of Inorganic and Coordination Compounds*; John Wiley & Sons, Inc.: New York, 1997.

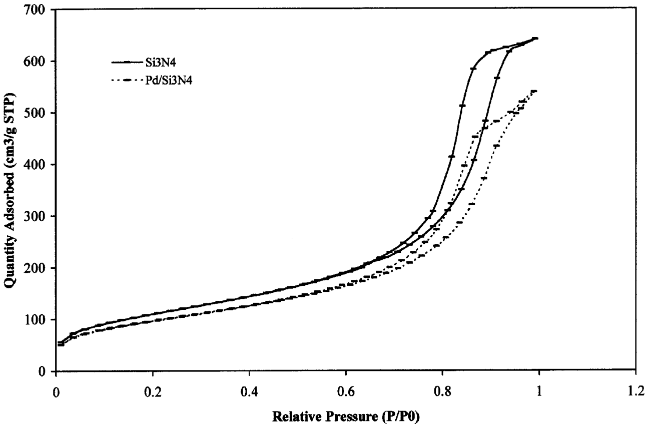

Figure 9. Nitrogen adsorption and desorption isotherms of the reduction product Pd/Si_3N_4−**3** from the precursor complex $Pd(DBA)_2$/Si_3N_4.

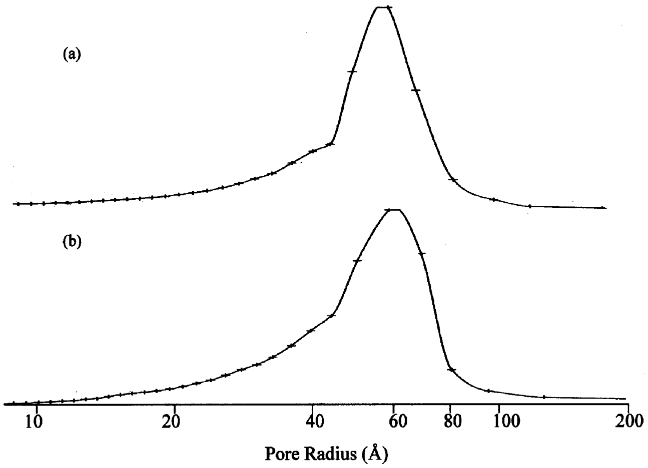

Figure 10. Pore size distribution of (a) Si_3N_4 and (b) the reduction product Pd/Si_3N_4−**3** from the precursor complex $Pd(DBA)_2$/Si_3N_4.

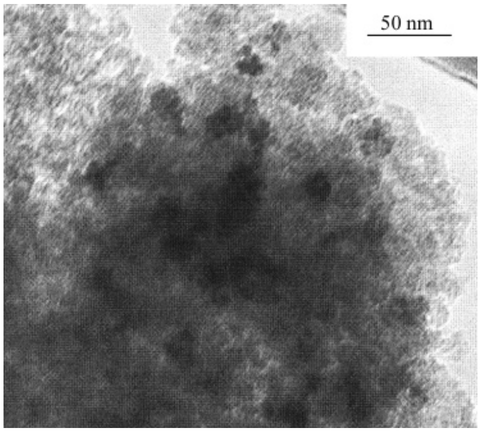

Figure 11. TEM of the reduction product Pd/Si_3N_4−**3** from the precursor complex $Pd(DBA)_2$/Si_3N_4.

similar size distributions and are crystalline or partially crystalline. The active surface area of these two catalysts is also similar in magnitude. The catalytic properties of the ceramics Pd/Si_3N_4−**1a** and −**1b** prepared by method 1 using a heating rate of 5 °C min^{-1} were not investigated because of the presence of two pore size distributions and a lower active surface area than that of the catalyst Pd/Si_3N_4−**1c** prepared by method 1 using a heating rate of 2 °C min^{-1}. In general, for samples Pd/Si_3N_4−**1a**, −**1b**, and −**1c**, where palladium is introduced directly into the gel, a nonnegligible amount of the palladium metal will also be located in the walls, which will not be accessible to reactants and will also reduce the catalysis activity. The catalyst Pd/Si_3N_4−**3**, prepared by method 3 involving the reduction of $Pd(dba)_2$, exhibits the lowest surface area and smallest concentration of palladium nanoclusters. However, the palladium nanoclusters are amorphous solids and the diameter is much smaller than those present on the catalysts Pd/Si_3N_4−**1c** and Pd/Si_3N_4−**2**.

Hydrogenation Reactions. One of the most important reactions in heterogeneous metal catalysis is the catalytic hydrogenation of alkene and carbonyl groups. In order to investigate and compare the catalytic activity of the Pd/Si_3N_4−**1c**, −**2**, and −**3** nanocomposites prepared using the three different chemical routes 1−3, we performed a preliminary investigation of the catalytic hydrogenation of 1-hexene and cyclohexanone. Tables 4 and 5 summarize the reaction conditions and degree of conversion to the desired products.

The hydrogenation of hex-1-ene was carried out at 30 °C under 40 psi for 4 h. The hydrogenation of cyclohexanone was carried out at 135 °C under 30 psi for 12 h. Table 4 shows that when the ceramic Pd/Si_3N_4−**1c** (prepared from silicon diimide gel and $PdCl_2$) was used as a catalyst, 16.4% of hex-1-ene was converted to hexane and 14.1% was converted to a mixture of (*Z*)-hex-2-ene and (*E*)-hex-2-ene. When the ceramic Pd/Si_3N_4−**2** (prepared from silicon nitride and $PdCl_2$) was used as a catalyst, 80.7% of hex-1-ene was converted to hexane and 19.2% was converted to (*Z*)-hex-2-ene, and (*E*)-hex-2-ene. However, 100% of hex-1-ene was converted to hexane when the ceramic Pd/Si_3N_4−**3** (prepared from silicon nitride and $Pd(DBA)_2$) was used as a catalyst. Studies of the isomerization reaction of alkenes, such as hex-1-ene, catalyzed by Pd/Si_3N_4−**1c**, −**2**, and −**3** in the absence of hydrogen are ongoing. Pd/Si_3N_4−**1c** was also used to demonstrate hydrogenation at atmospheric pressure. 1-E-icosene was hydrogenated to eicosane at atmospheric pressure and room temperature in the presence of Pd/Si_3N_4−**1c** and hydrogen.

The conversion yields of cyclohexanone to cyclohexanol, as shown in Table 5, were 2.3, 11.7, and 55.6% for Pd/Si_3N_4−**1c**, −**2**, and −**3,** respectively. The low catalysis activity of Pd/Si_3N_4−**1c** is probably due to the fact that the crystalline palladium formed during the high-temperature processing is less active than the amorphous form. Pd/Si_3N_4−**3** has the highest catalysis activity probably, or at least in part, because the palladium nanoparticles are in an amorphous state and are smaller than those in Pd/Si_3N_4−**1c** and Pd/Si_3N_4−**2** and so have a higher effective surface area. Traces of chorine-containing impurities in catalysts Pd/Si_3N_4−**1c**, −**2**, and −**3** originating from the $PdCl_2$ added to the gel may also contribute to a lower catalytic activity.

The rate of conversion of cyclohexanone to cyclohexanol using the catalyst Pd/Si_3N_4−**3** is almost identical to that for the same reaction under almost identical reaction conditions with similar amounts of reagents and using palladium nanoparticles stabilized on silica (Pd/SiO_2) prepared in the same way as Pd/Si_3N_4−**3**.[48] The turnover frequency (TOF) appears to be almost an order of magnitude lower for the Pd/Si_3N_4−**3** catalyst because of an apparently higher loading

Table 3. Catalysts Pd/Si$_3$N$_4$−1c, −2, and −3 Prepared by Methods 1−3

ceramic	precursor	thermal treatment	atm	Pd (%)	Pd (nm)	area (m^2 g^{-1})
Pd/Si$_3$N$_4$−**1c**	5%-PdCl$_2$/Si(NH)$_2$	200−1000 °C @ 2 °C min^{-1}	NH$_3$	2.2	5−20	408
Pd/Si$_3$N$_4$−**2**	PdCl$_2$/Si$_3$N$_4$	350 °C	H$_2$	1.7	5−20	430
Pd/Si$_3$N$_4$−**3**	Pd(dba)$_2$/Si$_3$N$_4$	RT	H$_2$	0.8	5−10	346

Table 4. Hydrogenation of Hex-1-ene Using the Catalysts Pd/Si$_3$N$_4$−1c, −2, and −3 at 30 °C Under an Atmosphere of 40 psi H$_2$ for 4 h @ a [catalyst]/[substrate] Ratio of 1:17200

	conversion (%)		
catalyst	hexane	(*Z*)-hex-2-ene	(*E*)-hex-2-ene
Pd/Si$_3$N$_4$−**1c**	16.4	8.1	6.0
Pd/Si$_3$N$_4$−**2**	80.7	16.2	3.0
Pd/Si$_3$N$_4$−**3**	100		

Table 5. Hydrogenation of Cyclohexanone to Cyclohexanol Using the Catalysts Pd/Si$_3$N$_4$−1c, −2, and −3 at 135 °C Under an Atmosphere of 30 psi H$_2$ for 12 h @ a [catalyst]/[substrate] ratio of 1:12900

catalyst	conversion (%)
Pd/Si$_3$N$_4$−**1c**	2.3
Pd/Si$_3$N$_4$−**2**	11.7
Pd/Si$_3$N$_4$−**3**	55.6

of palladium, although the methods of preparation are almost identical.[48] The Pd/SiO$_2$ catalyst will be remade in our laboratories so that exact comparisons with similar palladium loadings and nanoparticle sizes can be made. However, there are indications that the Pd/Si$_3$N$_4$−**3** catalysts may be more active than catalysts where the palladium nanoclusters are supported on organic polymers or carbon.[47,48] More extensive studies of the efficiency of this type of catalyst prepared using method 3 are ongoing and will be reported in depth later. For example, we have successfully carried out some preliminary studies of the Heck reaction and are studying the Suzuki reaction using these new catalysts.

Conclusion

Three different nonaqueous sol−gel routes lead successfully to the synthesis of mesoporous silicon nitride with palladium nanoclusters distributed over the surface with different morphologies, i.e., highly crystalline Pd/α-S$_3$N$_4$, partially crystallized Pd/amorphous Si$_3$N$_4$ and amorphous Pd/Si$_3$N$_4$, with a high surface area and a narrow pore size distribution. The surface area and pore size distribution of the silicon nitride depend on the heating rate and final temperature of pyrolysis of the precursor gel to form the ceramic. A low heating rate was found to be most advantageous. Initial investigations of these nanocomposites indicate that they may be promising heterogeneous catalyts for a range of liquid-phase chemical reactions. Amorphous Pd/Si$_3$N$_4$ with small metal nanoclusters formed by an organometallic precursor route has the highest catalytic activity, whereas highly crystalline Pd/α-S$_3$N$_4$ formed by pyrolysis of a precursor gel incorporating the palladium metal is the least active form. The synthetic approach involving deposition of metal nanoclusters by reduction of an organometallic precursor on preformed silicon nitride appears the most attractive for catalysis applications.

Acknowledgment. Part of this work was carried out as part of the EU project NANOSENSOFLEX funded out of the GROWTH-G5RD-CT-2002-00722. The Engineering and Physical Sciences Research Council (EPSRC) of the United Kingdom provided further financial support. This financial support is gratefully acknowledged. We thank the Council for the Central Laboratory of the Research Councils (CCLRC) for access to synchrotron radiation and computing facilities at Daresbury Laboratory. We also thank Bob Knight for the ICP measurements. The reviewers are thanked for very helpful comments and suggestions.

CM061106H